Coherent O-band WDM Transmission of DP-16QAM over 50-km BDFA-Amplified Link

NATSUPA TAENGNOI,[1,2] KYLE R. H. BOTTRILL,[1,*] YANG HONG,[1,3] YU WANG,[1] JAYANTA SAHU,[1] LAJOS HANZO,[3] DAVID J. RICHARDSON,[1] AND PERIKLIS PETROPOULOS[1]

[1]*Optoelectronics Research Centre (ORC), University of Southampton, Southampton, SO17 1BJ, UK*
[2]*Currently with the Department of Electrical Engineering, Kasetsart University, Bangkok, 10900, Thailand*
[3]*Currently with Nokia Bell Labs, Paris-Saclay, Nozay, 91620, France*
[3]*School of Electronics and Computer Science, University of Southampton, Southampton, SO17 1BJ, UK*
**krhb1g12@soton.ac.uk*

Abstract: We present wavelength-division multiplexed coherent transmission in an O-band amplified link enabled by bismuth-doped fiber amplifiers (BDFAs). Transmission of 4×25 GBd DP-16QAM (4×200 Gb/s) is demonstrated over a single span of 50-km length, occupying a bandwidth of 4.7 THz across the wavelengths 1323 nm to 1351 nm.

1. Introduction

The demand for transmission capacity in intra/inter-datacenter interconnects is expected to keep growing, driven by high-definition video streaming services (for entertainment, business, and remote learning), big data, and telepresence. To meet this ever-growing demand, the development of solutions that utilize optical fibers more efficiently is necessary [1,2]. As a result, transmission in alternative bands is increasingly being explored [3–7], involving the development of a range of enabling technologies, including novel transmission fibers (such as multi-core [8,9] and nested anti-resonant nodeless hollow-core fibers [10,11]) and amplifiers (such as super-broadband semiconductor optical amplifiers [12], erbium-(co)doped fiber amplifiers for the C+L bands and extended L-band [13], and broadband Raman amplifiers [14]).

Among the six transmission bands commonly identified in silica fiber (O, E, S, C, L, and U), the O-band has a number of interesting features. Apart from the fact that technologies to support O-band transmission have, for a long time, been a staple in datacenter interconnects, the O-band also offers – (i) low-cost laser sources, (ii) very low chromatic dispersion (CD) compared to the C-band (even though this may present challenges in extended reach wavelength division multiplexed (WDM) transmission), (iii) sufficient wavelength separation from the C-band that no Raman interaction will occur between them. Combined with the emergence of the bismuth-doped phosphosilicate fiber amplifiers (BDFAs) in this region [15–17], the O-band has become a serious contender for adoption in multi-band transmission systems. In comparison, Praseodymium doped fiber amplifier solutions for O-band gain generally rely on more exotic glass hosts, such as fluoride glasses and chalcogenide glasses [18], which are costlier to manufacture and more difficult to handle than the phosphosilicate host of contemporary BDFAs. Similarly, Neodymium doped fiber amplifiers also rely on exotic glasses, such as Tellurite glass to enhance O-band efficiency [19]. Compared to semiconductor optical amplifiers (SOAs), BDFAs (and doped fiber amplifiers in general) offer superior linearity and generally superior noise figure performance as well [2,20].

There have been a number of demonstrations enabled by BDFAs for high-capacity single-channel and WDM transmission over recent years [3,21–24]. However, to date, most BDFA amplified O-band demonstrations have been performed using direct-detection (DD) formats,

the prevailing communication technology for short-haul optical communication. Although DD has, at least until now, continued to offer economic advantages over coherent communications, it is becoming ever more challenging to deliver increasing data rates on line cards with this technology [25]. To keep pace with increasing line rates, O-band coherent communication may be deployed in the future, partly due to the improved spectral efficiency they offer compared to DD. The rich digital signal processing (DSP) enabled by coherent detection offers a particular set of advantages to O-band communications. First of all, although still well within the transmission window of standard single-mode fiber (SMF), light in the O-band experiences approximately 0.1 dB/km additional loss when compared to the C-band; as a result, the additional sensitivity of coherent detection may be especially valuable when considering an extended transmission reach. At the same time, although the O-band is well-known for containing the zero-dispersion wavelength of SMF, CD is not entirely negligible in this band, particularly at the upper wavelength edge. For instance, deep power fading can affect signals with bandwidths beyond 17.5 GHz at 1360 nm after as little as 70 km of transmission in SMF [26]. In such circumstances, digital CD compensation may be implemented in DSP after coherent detection, potentially with reduced complexity than in the C-band and at a lower cost than optical CD compensation.

Although the reliance on DSP for many of these advantages may provoke concerns of high power consumption compared to comparatively DSP-light DD alternatives, it is interesting to note that high-capacity coherent communication may actually offer reduced power consumption in certain circumstances. In [27], it was predicted that a single carrier 1.6 Tbps coherent link would exhibit reduced power consumption relative to an 8×200-Gbps DD link, a 4×400-Gbps DD link, as well as a 2×800-Gbps coherent link. Delivering the high datarates necessary to show such benefits will rely on leveraging the latest advances in electronic and photonic technologies, such as application-specific integrated circuits (ASICs) and high-bandwidth thin-film lithium niobate-based devices [28]. Recent activity surrounding the 400G-ZR standard and the move towards coherent pluggable technologies is a promising development for the adoption of coherent O-band communication as it is potentially an indicator of improved cost-effectiveness of modern coherent receiver fabrication, further motivating this study [29].

On the one hand, optical nonlinearity is expected to impact O-band transmission more than C-band transmission, not only because the nonlinear coefficient [30] is greater in the former, but also because the reduced CD has a lesser suppressive effect on nonlinear four-wave mixing. Attempts have been made to suppress the impact of nonlinearity in the O-band; in [31,32], an alternating-phase format was proposed to alleviate nonlinearity in DD transmission. Owing at least to their increased power efficiency (energy per bit) compared to DD formats, coherent formats generally show a later onset of nonlinear impairments for the same data rate [33].

The Gaussian-Noise (GN) model [34] can be used to shed light on the impact of dispersion on O-band performance. Considering a link consisting of homogenous spans of SMF-28 with inline lumped amplification and a transmission band consisting of many (sufficient to use the locally-white noise approximation [34]) identical, equispaced signals, the results of [34] can be used to derive the following equation, describing the expected reach, N_S^{max} (in terms of maximum spans) of a transmission band centred at a wavelength λ, relative to the reach of as otherwise identical band centered at 1550 nm (more details are provided in Appendix):

$$\frac{N_S^{max}(\lambda)}{N_S^{max}(1550)} = \sqrt[3]{\frac{\alpha_{dB}(1550\text{nm})\,\gamma^2(1550\text{nm})\,L_{eff}^2(1550\text{nm})\,|D(\lambda)|}{\alpha_{dB}(\lambda)\,\gamma^2(\lambda)\,L_{eff}^2(\lambda)|D(1550\text{nm})|}} \quad (1)$$

Where α_{dB} is the attenuation of the transmission fiber (in decibels per unit length), γ is its nonlinear coefficient, L_{eff} is its effective length and D is its dispersion. This unitless estimator of relative reach is plotted with a solid line on the in Fig. 1, using parameters appropriate for

SMF-28 (more details are provided in Appendix). We have identified, with a dashed line, a region of higher uncertainty (corresponding to $D < 1\ ps/nm \cdot km$) about the zero-dispersion wavelength of 1310 nm and supplemented the graph with a plot of chromatic dispersion (dotted line, right axis). Even with this uncertainty about the zero-dispersion wavelength in mind, it is clear that the maximum expected reach of a WDM transmission in the O-band is highly sensitive to chromatic dispersion and suggests that pushing transmission to the upper wavelength region of the O-band should deliver improved nonlinear performance relative to transmission about the zero-dispersion wavelength.

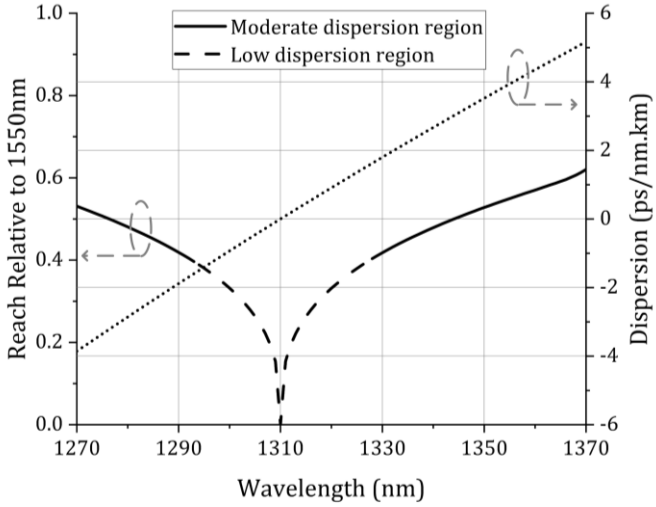

Fig. 1. GN model estimated reach in O-band compared to at 1550 nm.

In terms of recent experimental activity in the O-band, a single-channel dual-polarization 64-ary quadrature amplitude modulation (DP-64QAM) transmission at 1310 nm was demonstrated [23], carrying up to 1.6 Tb/s over 10 km. This transmission was enabled by utilizing a thin-film lithium niobate IQ modulator and a praseodymium-doped fiber amplifier. Additionally, in [24], a 40-GBd 16-QAM WDM O-band transmission system was demonstrated over a notably wide bandwidth of 9.6 THz, using BDFAs to support a reach of 135 km (utilizing three 45-km spans of fiber). It is noteworthy that the authors of [24] observed some penalties due to nonlinearity at the short wavelength edge of the spectrum, around the zero-dispersion wavelength of the transmission fiber.

In the present study, we experimentally demonstrate BDFA-enabled coherent O-band transmission utilizing the upper wavelength region of the O-band (specifically, between 1323 nm to 1351 nm), benefitting from relatively high CD values compared to lower wavelength regions, which suppresses four-wave mixing and mitigates the effects of cross-phase modulation [35]. Four channels with a DP-16QAM were transmitted with a baud rate of 25 GBd (200 Gb/s/λ). The channels were spaced across a 4.7-THz bandwidth, between 1323-1351 nm. The performance of the four channels after transmission showed that no error floor can be detected (without using forward error correction). This paper extends the work presented at the Optical Fiber Communication Conference (OFC) 2023 conference [36].

2. Experimental setup and coherent signal generation

Fig. 2 shows the setup of the full transmission link. The WDM transmission system presented in this paper consisted of four channels, which were coarsely distributed across the gain region of the BDFAs [15] used in the experiment. The four channels were located at the wavelengths of 1323, 1331, 1343, and 1351 nm. To form these WDM channels, two branches of signal

generators were used at the transmitter to generate: (i) the channel-under-test (CUT), tuned to the wavelength of interest and (ii) the remaining dummy channels (one of which was replaced by the CUT). These branches were simultaneously modulated with 25-GBd DP-16QAM during the measurement (note that the receiver sample rate of 40 GSa/s prevented the baudrate from being increased much beyond 25 GBd without compromising performance). This approach was used in the transmitter due to the limited availability of lasers with suitable linewidth for successful coherent detection; the CUT used a tunable laser with a narrow linewidth of 200 kHz, whilst the WDM dummy channel lasers consisted of fixed-wavelength distributed feedback lasers with a relatively broad linewidth (several MHz). The broad carrier linewidth used to generate the dummy channels was not a concern since only the CUT was evaluated at the receiver. To characterize the behavior of the system at all four studied channels, the CUT wavelength was re-tuned to the appropriate wavelength and the corresponding dummy channel was deactivated (effectively being replaced by the CUT).

It was found that the IQ modulators available for the experiment, which were all designed for operation in the C/L-band, exhibited a compromised extinction ratio in the O-band. Again, this was not a concern for the dummy channels. These were generated by first multiplexing their carrier lasers and then modulating them with the same IQ modulator, as commonly done. To decorrelate the data of neighboring WDM channels, the signals at 1331 nm and 1351 nm were demultiplexed from the signals at 1323 nm and 1343 nm and propagated over different length delay lines before being re-multiplexed. An O-band semiconductor optical amplifier (SOA) was used to compensate for the loss of this decorrelation step (the two BDFAs available were reserved for use in the transmission link and so one was not available here).

For the CUT, however, we identified a dual-drive C-band Mach-Zehnder Lithium Niobate modulator (DD-MZM) with acceptable O-band performance and so this was used instead. As the modulator was a simple MZM rather than an IQ-modulator, a technique of amplitude modulation followed by optical quadrature multiplexing was adopted: Firstly, a 4-level bipolar amplitude-shift keying (ASK) signal was created on one quadrature by driving the DD-MZM with a symmetric 4-level signal from an arbitrary waveform generator. The inset of Fig. 2 shows the constellation diagrams associated with this step. Next, this signal was launched into an optical delay line interferometer (DLI), which, by coherently combining the 4-level ASK signal with a delayed version of itself, was able to generate the 25-GBd 16QAM signal desired.

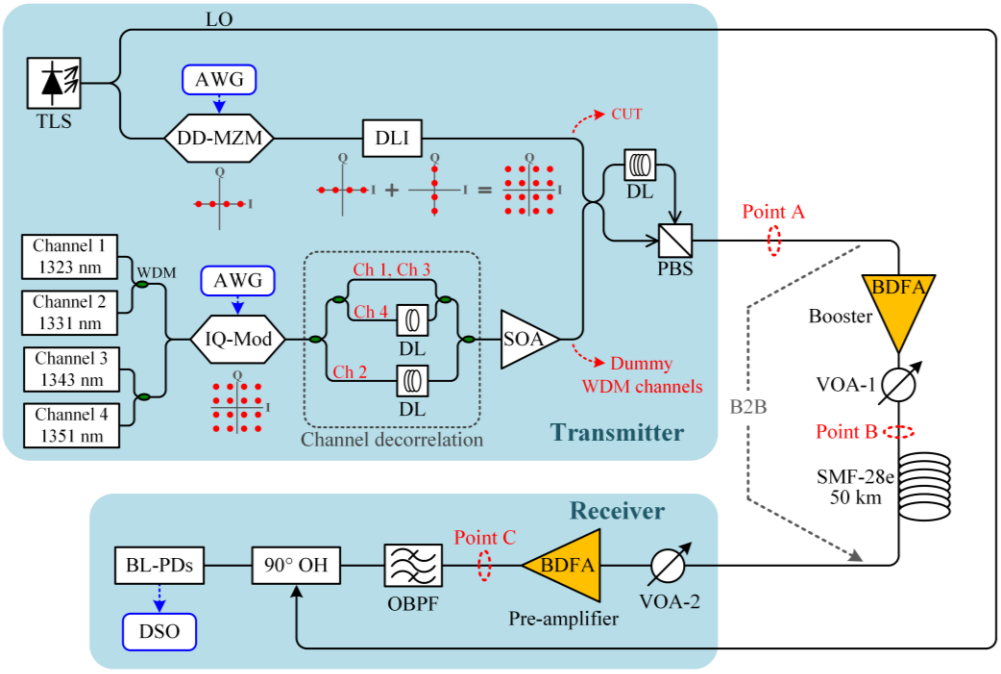

AWG = arbitrary waveform generator
BL-PDs = balanced photodiodes
DL = delay line
DLI = delay line interferometer
DSO = digital storage oscilloscope
LO = local oscillator
MUX = multiplexer
OBPF = optical bandpass filter
PBS = polarization beam splitter
SOA = semiconductor optical amplifier
TLS = tunable laser source
VOA = variable optical attenuator
90° OH = 90-degree optical hybrid

Fig. 2. Experimental setup of the DP-16QAM WDM transmission over 50-km amplified link with illustrations of constellation diagrams inset for the modulation steps.

The resulting 16QAM signals from the CUT branch and the dummy branch were then combined by a 3-dB polarization-maintaining coupler, creating a single-polarization, four-channel WDM band. In order to obtain polarization multiplexed signals, a polarization beam splitter (PBS) was subsequently used to orthogonally re-multiplex the two outputs of the coupler. By using length-mismatched sections of fiber to connect the coupler to the PBS, a relative delay of ~48 symbols between the two multiplexed polarizations was applied, to ensure that their data streams were decorrelated.

The 25-GBd DP-16QAM WDM band was then amplified using a BDFA (booster) [15] with ~20-dB gain, 16-dBm saturated output power, and ~6.5-dB averaged noise figure (NF) measured across the tested wavelength range. Further characterization details of a very similar BDFA can be found in [20]. The powers of all channels were leveled before launching them into the transmission fiber by adjusting the optical power of the carrier lasers as appropriate, because the BDFA had no gain flattening filter. Fig. 3 shows the spectra measured at various locations in the link. The total launch power was adjustable via a variable optical attenuator (VOA-1). The transmission fiber was a 50-km length of SMF-28e. The measured loss of the fiber was ~0.3 dB/km at 1310 nm.

At the receiver, the signal power was amplified by a second BDFA (pre-amplifier) with a gain of ~26 dB, whilst the optical signal-to-noise ratio (OSNR) of the signal was controllable using VOA-2. Subsequently, the CUT was selected out using an optical bandpass filter with a 20-dB bandwidth of 1.2 nm, before being detected using a custom-made, O-band optimized 90-degree optical hybrid (90° OH) whose local oscillator (LO) was fed from the same laser used for the CUT (i.e., homodyne detection was employed). Afterward, a set of four balanced

photodiodes was used to detect the outputs of the optical hybrid. The outputs of the photodiodes were connected to a digital storage oscilloscope with a 40-GSa/s sample rate and their waveforms were digitized for digital signal processing and demodulating, to obtain bit-error ratio (BER) measurements via error counting.

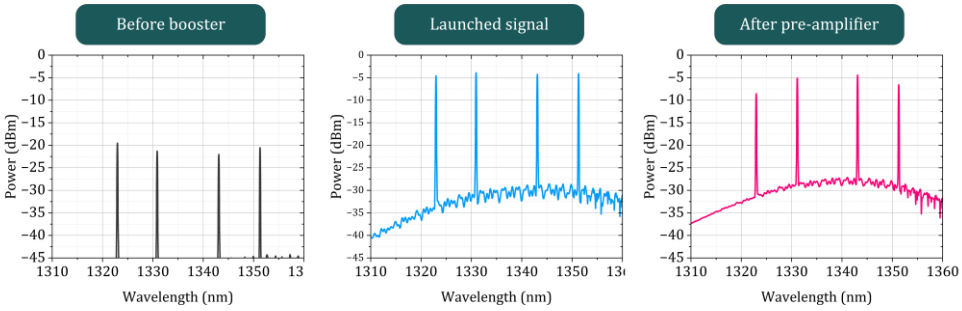

Fig. 3. Optical spectra measured before booster (point A), launched signal for the 6 dBm total power condition (point B), and after pre-amplifier (point C) by using OSA resolution of 0.1 nm.

3. Transmission results and discussion

To determine the optimum launch power of the WDM transmission, the BER was measured at each wavelength after transmission by sweeping the total power launched into the fiber using VOA-1. The results are shown in Figs. 4(a) - 4(d), for each channel, with power varied over a launch power range of -1.5 - 6 dBm, which corresponded approximately to a received power between -16.5 dBm and -9 dBm. BERs lower than the 7% hard-decision forward-error-correction (HD-FEC) threshold of 3.8×10^{-3} (indicated by the dashed line on the plots) were achieved after 50-km transmission, for all channels. Meanwhile, the optimum total launch power for all channels, which was identified as the power resulting in the lowest BER, was shown to be around 4-5 dBm, beyond which the signal quality degraded due to optical nonlinearities. The shortest-wavelength channel shown in Fig. 4(a) performed worse than the others as it required higher launch power to reach the best BER. This is likely due to a combination of the BDFAs providing less gain and higher noise figure at the shorter wavelengths compared to the longer wavelengths (see [20] for a characterization of the BDFAs used in this work) as well as the wavelength-dependent extinction ratio of the MZM modulator used to generate the signal, as this was designed for the C-band.

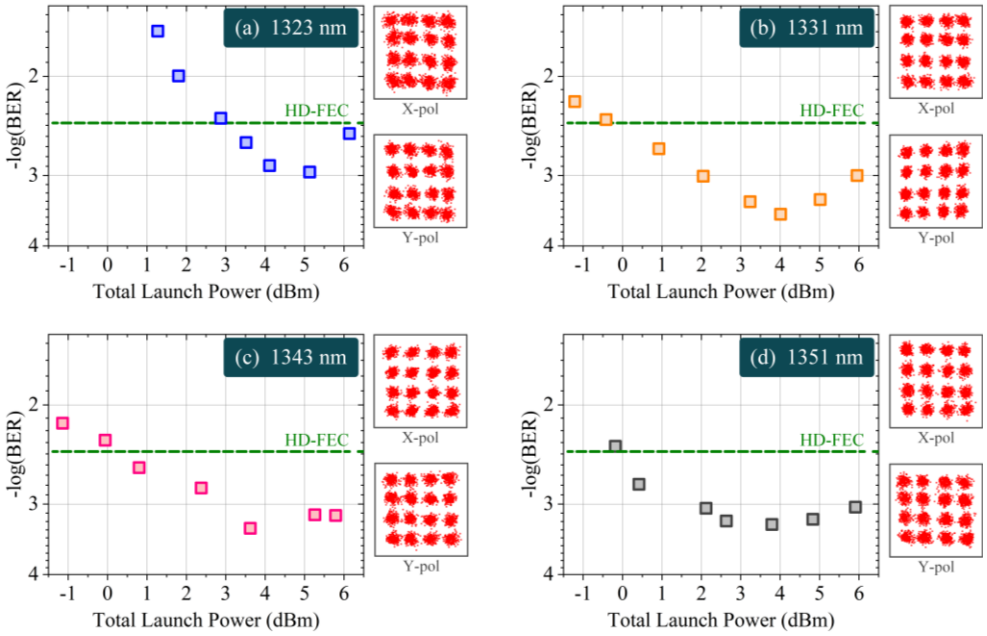

Fig. 4. BER results versus total launch power with constellation diagram insets for (a) 1323 nm, (b) 1331 nm, (c) 1343 nm, and (d) 1351 nm.

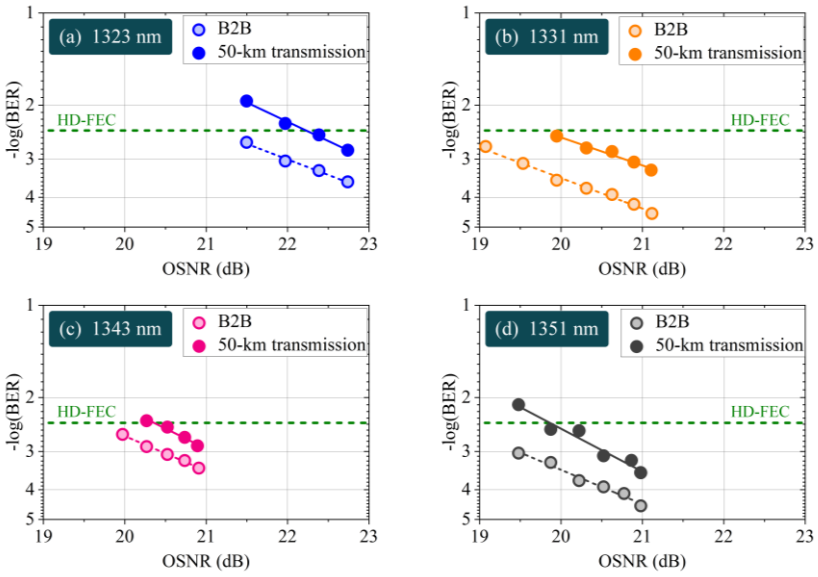

Fig. 5. BER results when varying the OSNR for both B2B and after 50-km transmission with linear-fit lines of the data for (a) 1323 nm, (b) 1331 nm, (c) 1343 nm, and (d) 1351 nm.

As our objective was to demonstrate WDM transmission, for further testing, it was necessary to ensure that all channels could comfortably exceed the 7% HD-FEC limit simultaneously (i.e., at the same constant launch power). As such, the launch power was selected to favor the wavelength with the worst sensitivity: 1323 nm (see Figs. 4(a) - 4(d)). Hence, a total launch power of 5 dBm was selected, with the consequence that, although all channels comfortably exceeded the 7% HD-FEC limit, wavelengths 1331 nm, 1343 nm, and

1351 nm were transmitted at a power slightly beyond their optimum and hence suffered from a small nonlinear degradation.

The constellation diagrams of the X and Y polarizations of the DP-16QAM signal at each wavelength taken at 5-dBm total launch power are presented in the insets to Figs. 4(a) - 4(d). The penalty of each channel after 50-km transmission was studied next by sweeping the received signal's OSNR using VOA-2. The BER results are presented in Figs. 5(a) - 5(d), for each channel, along with their BERs before transmission (back-to-back, B2B) for comparison. The B2B is indicated by the dashed line bypassing the booster BDFA and transmission fiber that form the transmission link in Fig. 2. After transmission, there is no evidence of an error floor at the error levels measured for any of the channels tested, although there is an OSNR penalty (defined as the additional OSNR required after transmission to deliver a given BER compared to B2B). This penalty arises from our choice to operate in the nonlinear regime to ensure all wavelengths were detectable below the 7% HD-FEC limit.

4. Conclusions

We demonstrated a coherent O-band WDM transmission consisting of four 25 GBd (200 Gb/s/λ) DP-16QAM signals. Amplification was achieved with two in-house built BDFAs that provided a transmission bandwidth of 4.7 THz (between 1323-1351 nm). This work shows the potential for the BDFA to enable the high-capacity transmission afforded by higher-order modulation formats, such as DP-16QAM, in the O-band. In future work, we aim to extend the overall transmission reach further, as we work towards demonstrating high-capacity, moderate reach DWDM transmission in the O-band.

5. Appendix

The basis for the analytical results presented in Eq. 1 are the results obtained in [34] for a link consisting of homogenous spans, with inline lumped amplification and a transmission band consisting of identical, equispaced signals. The 'maximum system reach', the maximum number of spans a transmission is predicted to travel and maintain acceptable system performance, is given as 'Eq. (55)' in [34] as:

$$N_S^{max} = \frac{1}{3\,SNR_T}\sqrt[3]{\frac{4}{\left(P_{ASE}^{1\,span}\right)^2 \cdot \eta^{1\,span}}} \tag{A1}$$

where SNR_T is the target signal-to-noise-ratio at the receiver, $P_{ASE}^{1\,span}$ is the amplified spontaneous emission noise due to the lumped amplification at the end of each span. $\eta^{1\,span}$ is defined as $\eta^{1\,span} = P_{ASE}^{1\,span}/P_{ch}^3$, where P_{ch} is the average power per channel (raised to the third power). A closed form approximation for $\eta^{1\,span}$ is provided in [34] as:

$$\eta^{1\,span} \approx C\,\frac{R_S}{\Delta f_{ch}}\,\frac{\alpha_{dB}\gamma^2 L_{eff}^2}{|D|R_S^2} \tag{A2}$$

where C is a constant (which will be eliminated), R_S is the symbol rate of the transmission and, importantly, $\alpha_{dB}$is the (decibel) loss per unit length of the transmission fiber, γ is its nonlinear coefficient, $L_{eff}$is its effective length and D is its dispersion.

Combining Eqs. (A1) and (A2), the following equation can be obtained (note the explicit wavelength, λ, dependency we have included):

$$N_S^{max}(\lambda) = \frac{1}{3}\sqrt[3]{\frac{4}{\left(P_{ASE}^{1\ span}\right)^2 C\,\frac{R_S}{\Delta f_{ch}}\,\frac{\alpha_{dB}(\lambda)\,\gamma^2(\lambda)\,L_{eff}^2(\lambda)}{|D(\lambda)|R_S^2}}} \tag{A3}$$

For our purposes, we wish only to determine the trend in performance as the transmission wavelength approaches the zero-dispersion wavelength of SMF28. To maintain generality, we consider the relative performance (in terms of maximum system reach) of transmission at a wavelength of λ compared to a transmission in the C-band at 1550 nm. This value is chosen not only for familiarity but importantly because, given the GN model's assumption that the impact of nonlinearity is equivalent to an additive Gaussian noise, the above results suffer from increased uncertainty for low values of dispersion, where signals better maintain their original pulse shape during propagation and remain statistically non-Gaussian. Dividing $N_S^{max}(\lambda)$ by $N_S^{max}(\lambda = 1550\ \text{nm})$ and setting SNR_T, $P_{ASE}^{1\ span}$, C, R_S and Δf_{ch} to be constant with λ (we only wish to study the effects of dispersion and nonlinearity), we obtain:

$$\frac{N_S^{max}(\lambda)}{N_S^{max}(1550\text{nm})} = \sqrt[3]{\frac{\alpha_{dB}(1550\text{nm})\,\gamma^2(1550\text{nm})\,L_{eff}^2(1550\text{nm})}{|D(1550\text{nm})|}\,\frac{|D(\lambda)|}{\alpha_{dB}(\lambda)\,\gamma^2(\lambda)\,L_{eff}^2(\lambda)}} \tag{A4}$$

Fig. 6 provides plots of the attenuation, dispersion and nonlinear coefficient data used in the calculation of $N_S^{max}(\lambda)/N_S^{max}(1550\text{nm})$ in Fig. 1 using Eq. 1 (Eq. A4).

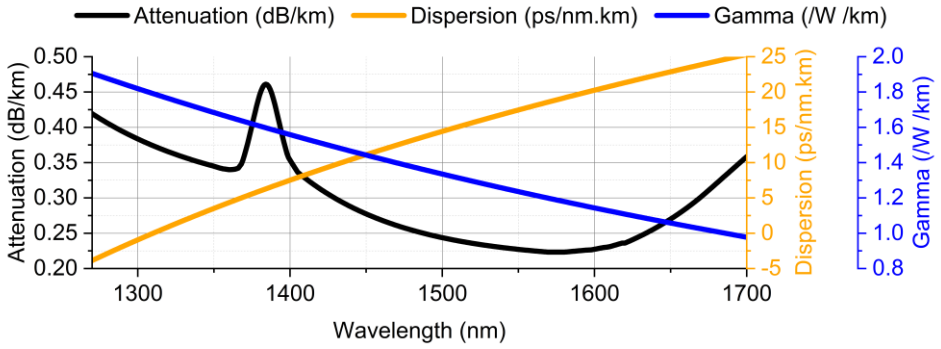

Fig. 6. Plots of the attenuation, dispersion and nonlinear coefficient curves used in the calculation of $N_S^{max}(\lambda)/N_S^{max}(1550\text{nm})$ in Fig. 1 using Eq. 1 (Eq. A4).

Funding. Engineering and Physical Sciences Research Council (EP/P030181/1, EP/P003990/1, EP/X04047X/1, EP/X040569/1 and EP/X030040/1). DCIT (project REASON).

Disclosures. The authors declare no conflicts of interest.

Data availability. Open access data for this work is available at doi:10.5258/SOTON/XXXXXX.

References

1. P. J. Winzer, D. T. Neilson, and A. R. Chraplyvy, "Fiber-optic transmission and networking: the previous 20 and the next 20 years [Invited]," Opt. Express **26**(18), 24190-24239 (2018).
2. L. Rapp and M. Eiselt, "Optical Amplifiers for Multi–Band Optical Transmission Systems," J. Light. Technol. **40**(6), 1579-1589 (2022).

3. N. Taengnoi, K. R. H. Bottrill, N. K. Thipparapu, A. A. Umnikov, J. K. Sahu, P. Petropoulos, and D. J. Richardson, "WDM Transmission with In-Line Amplification at 1.3μm Using a Bi-Doped Fiber Amplifier," J. Light. Technol. **37**(8), 1826-1830 (2019).
4. Y. Hong, T. Bradley, N. Taengnoi, K. R. H. Bottrill, J. Hayes, G. Jasion, F. Poletti, P. Petropoulos, and D. J. Richardson, "Hollow-Core NANF for High-Speed Short-Reach Transmission in the S+C+L-Bands," J. Light. Technol. **39**(19), 6167-6174 (2021).
5. N. Taengnoi, K. R. H. Bottrill, Y. Hong, L. Hanzo, and P. Petropoulos, "Ultra-Long-Span U-Band Transmission Enabled by Incoherently Pumped Raman Amplification," J. Light. Technol. **41**(12), 3767-3773 (2023).
6. D. Soma, T. Kato, S. Beppu, D. J. Elson, H. Muranaka, H. Irie, S. Okada, Y. Tanaka, Y. Wakayama, N. Yoshikane, T. Hoshida, and T. Tsuritani, "25-THz O+S+C+L+U-Band Digital Coherent DWDM Transmission Using a Deployed Fibre-Optic Cable," in *Proc. of ECOC* (IET, 2023), paper Th.C.2.2.
7. B. Puttnam, R. Luis, Y. Huang, I. Phillips, D. Chung, N. Fotaine, G. Rademacher, M. Mazue, L. Dallachiesa, H. Chen, W. Forysiak, R. Man, R. Ryf, D. Nielson, and H. Furukawa, "301 Tb/s E, S, C+L-Band Transmission over 212 nm bandwidth with E-band Bismuth-Doped Fiber Amplifier and Gain Equalizer," in *Proc. of ECOC* (IET, 2023), paper Th.C.2.4.
8. D. L. Butler, "Space-Division Multiplexing (SDM) Technology for Short Reach Fiber Optic Systems," in *Proc. of OFC* (Optica, 2016), paper Tu3I.1.
9. S. Beppu, H. Takahashi, T. Gonda, K. Imamura, K. Watanabe, R. Sugizaki, and T. Tsuritani, "56-Gbaud PAM4 Transmission over 2-km 125-μm-Cladding 4-Core Multicore Fibre for Data Centre Communications," in *Proc. of ECOC* (IEEE, 2017), paper Th.2.A.2.
10. H. Sakr, K. R. H. Bottrill, N. Taengnoi, N. V. Wheeler, P. Petropoulos, D. J. Richardson, F. Poletti, Y. Hong, T. Bradley, G. T. Jasion, J. Hayes, H. Kim, I. Davidson, E. N. Fokoua, and Y. Chen, "Interband Short Reach Data Transmission in Ultrawide Bandwidth Hollow Core Fiber," J. Light. Technol. **38**(1), 159-165 (2020).
11. Y. Hong, K. R. H. Bottrill, T. D. Bradley, H. Sakr, G. T. Jasion, K. Harrington, F. Poletti, P. Petropoulos, and D. J. Richardson, "Low-Latency WDM Intensity-Modulation and Direct-Detection Transmission Over >100 km Distances in a Hollow Core Fiber," Laser Photonics Rev. **15**(9), 2100102 (2021).
12. J. Renaudier and A. Ghazisaeidi, "Scaling Capacity Growth of Fiber-Optic Transmission Systems Using 100+nm Ultra-Wideband Semiconductor Optical Amplifiers," J. Light. Technol. **37**(8), 1831-1838 (2019).
13. Z. Zhai and J. K. Sahu, "Extending L-Band Gain to 1625 nm Using Er^{3+}:Yb^{3+} Co-Doped Silica Fibre Pumped by 1480 nm Laser Diodes," in *Proc. of ECOC* (IEEE, 2022), paper Th2A.2.
14. M. A. Iqbal, L. Krzczanowicz, I. D. Phillips, P. Harper, A. Lord, and W. Forysiak, "Ultra-Wideband Raman Amplifiers for High Capacity Fibre-Optic Transmission Systems," in *Proc. of ICTON* (IEEE, 2020), paper Th.B6.4.
15. N. K. Thipparapu, A. Umnikov, P. Barua, and J. K. Sahu, "Bi-doped fiber amplifier with a flat gain of 25 dB operating in the wavelength band 1320–1360 nm," Opt. Lett. **41**(7), 1518-1521 (2016).
16. N. K. Thipparapu, Y. Wang, S. Wang, A. A. Umnikov, P. Barua, and J. K. Sahu, "Bi-doped fiber amplifiers and lasers [Invited]," Opt. Mater. Express **9**(6), 2446-2465 (2019).
17. V. Mikhailov, M. A. Melkumov, D. Inniss, A. M. Khegai, K. E. Riumkin, S. V. Firstov, F. V. Afanasiev, M. F. Yan, Y. Sun, J. Luo, G. S. Puc, S. D. Shenk, R. S. Windeler, P. S. Westbrook, R. L. Lingle, E. M. Dianov, and D. J. DiGiovanni, "Simple Broadband Bismuth Doped Fiber Amplifier (BDFA) to Extend O-band Transmission Reach and Capacity," in *Proc. of OFC* (Optica, 2019), paper M1J.4.
18. D. W. Hewak, "Progress towards a 1300 nm fibre amplifier," in *IEE Colloquium on New Developments in Optical Amplifiers (Ref. No. 1998/492)*, London, UK, 1998.
19. Z. Zi-zhong, Z. Ming-han, S. Xiu-e, P. Cheng, and Z Yaxun, "Enhanced 1.32 μm fluorescence and broadband amplifying for O-band optical amplifier in Nd^{3+}-doped tellurite glass," Optoelectron. Lett. **13**(1), 54-57 (2017).
20. N. Taengnoi, K. R. H. Bottrill, Y. Hong, Y. Wang, N. K. Thipparapu, J. K. Sahu, P. Petropoulos, and D. J. Richardson, "Experimental characterization of an O-band bismuth-doped fiber amplifier," Opt. Express **29**(10), 15345-15355 (2021).
21. M. S. B Hossain, J. Wei, F. Pittalà, N. Stojanović, S. Calabrò, T. Rahman, G. Böcherer, T. Wettlin, C. Xie, M. Kuschnerov, and S. Pachnicke, "402 Gb/s PAM-8 IM/DD O-Band EML Transmission," in *Proc. of ECOC* (IEEE, 2021), paper We1C1.4.

22. Y. Hong, N. Taengnoi, K. R. H. Bottrill, N. K. Thipparapu, Y. Wang, J. K. Sahu, D. J. Richardson, and P. Petropoulos, "Experimental demonstration of single-span 100-km O-band 4×50-Gb/s CWDM direct-detection transmission," Opt. Express **30**(18), 32189-32203 (2022).

23. E. Berikaa, M. S. Alam, S. Bernal, W. Li, B. Krueger, F. Pittalà, and D. V. Plant, "Net 1.6 Tbps O-band Coherent Transmission over 10 km Using a TFLN IQM and DFB Lasers for Carrier and LO," in *Proc. of OFC* (Optica, 2023), paper Th4B.1.

24. D. J. Elson, Y. Wakayama, V. Mikhailov, J. Luo, N. Yoshikane, D. Inniss, and T. Tsuritani, "9.6-THz Single Fibre Amplifier O-band Coherent DWDM Transmission," in *Proc. of OFC* (Optica, 2023), paper Th4B.4.

25. X. Zhou, R. Urata, and H. Liu, "Beyond 1Tb/s Datacenter Interconnect Technology: Challenges and Solutions [Invited]," in *Proc. of OFC* (Optica, 2019), paper Tu2F.5.

26. Y. Hong, K. R. H. Bottrill, N. Taengnoi, N. K. Thipparapu, Y. Wang, J. K. Sahu, D. J. Richardson, and P. Petropoulos, "Numerical and experimental study on the impact of chromatic dispersion on O-band direct-detection transmission," Appl. Opt. **60**(15), 4383-4390 (2021).

27. E. Berikaa, M. S. Alam, S. Bernal, R. Gutiérrez-Castrejón, W. Li, Y. Hu, B. Krueger, F. Pittalà, and D. V. Plant, "Next-Generation O-Band Coherent Transmission for 1.6 Tbps 10 km Intra-Datacenter Interconnects," J. Light. Technol. **42**(3), 1126-1135 (2024).

28. E. Berikaa, M. D. Alam, W. Li, S. Bernal, B. Krueger, F. Pittalà, D. V. Plant, "TFLN MZMs and Next-Gen DACs: Enabling Beyond 400 Gbps IMDD O-Band and C-Band Transmission," IEEE Photonics Technol. Lett. **35**(15), 850-853 (2023).

29. P. M. Seiler, G. Georgieva, G. Winzer, A. Peczek, K. Voigt, S. Lischke, A. Fatemi, and L. Zimmermann, "Toward coherent O-band data center interconnects," Front. Optoelectron. **14**(4), 414–425 (2021).

30. T. Sato, S. Makino, Y. Ishizaka, T. Fujisawa, and K. Saitoh, "A rigorous definition of nonlinear parameter γ and effective area A_{eff} for photonic crystal optical waveguides," JOSA B **32**(6), 1245-1251 (2015).

31. N. Taengnoi, K. R. H. Bottrill, C. Lacava, D. J. Richardson, and P. Petropoulos, "AMI for Nonlinearity Mitigation in O-Band Transmission," in *Proc. of OFC* (Optica, 2019), paper Th2A.33.

32. N. Taengnoi, K. R. H. Bottrill, Y. Hong, N. Thipparapu, C. Lacava, J. K. Sahu, D. J. Richardson, and P. Petropoulos, "4-level Alternate-Mark-Inversion for Reach Extension in the O-band Spectral Region," J. Light. Technol. **39**(9), 2847-2853 (2021).

33. E. Ip, A. P. T. Lau, D. J. F. Barros, and J. M. Kahn, "Coherent detection in optical fiber systems," Opt. Express **16**(2), 753-791 (2008).

34. P. Poggiolini, G. Bosco, A. Carena, V. Curri, Y. Jiang, and F. Forghieri, "The GN-Model of Fiber Non-Linear Propagation and its Applications," J. Light. Technol. **32**(4), 694-721 (2014).

35. P. J. Winzer and R. Essiambre, "Advanced Optical Modulation Formats," Proc. IEEE **94**(5), 952-985 (2006).

36. N. Taengnoi, K. R. H. Bottrill, Y. Hong, Y. Wang, J. Sahu, L. Hanzo, D. J. Richardson, and P. Petropoulos, "Coherent O-band Transmission of 4×25 GBd DP-16QAM Channels Over a 50 km BDFA-Equipped Link," in *Proc. of OFC* (Optica, 2023), paper Th3F.5.